Using CRISPR barcoding as a molecular clock to capture dynamic processes at single-cell resolution

Yolanda Andres-Lopez†[1], Alice Santambrogio†[2,3], Ioannis Kafetzopoulos†[2,3], Christopher Todd[2,3], Carla El Khouri[1], Celia Alda-Catalinas[2,4], Stephen J. Clark[2,3], Wolf Reik*[2,3] & Irene Hernando-Herraez*[2,1]

[1] Instituto de Biología Molecular de Barcelona, Consejo Superior de Investigaciones Científicas (IBMB-CSIC), Barcelona, 08028, Spain

[2] Epigenetics Programme, Babraham Institute, Cambridge, CB22 3AT, United Kingdom

[3] Altos Labs, Granta Park, Cambridge, CB21 6GQ, United Kingdom

[4] Genomic Sciences, GSK, Stevenage, SG1 2NFX, United Kingdom

* To whom correspondence should be addressed: wreik@altoslabs.com and ihhbmc@ibmb.csic.es

† Joint Authors

GRAPHICAL ABSTRACT

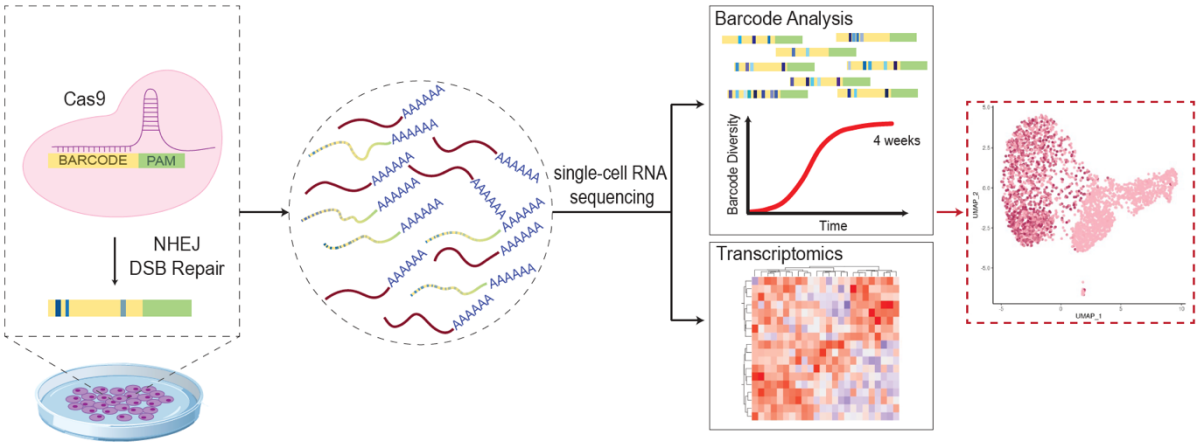

ABSTRACT

Biological processes are fundamentally dynamic, yet existing methods for capturing these temporal changes are limited. We present scDynaBar, a novel approach that integrates CRISPR-Cas9 dynamic barcoding with single-cell sequencing to enable the recording of temporal cellular events. In this system, genetic barcodes accumulate mutations over a 25-day period and then are sequenced together with the transcriptome of each single cell. We propose that this gradual accumulation of genetic diversity can be exploited to create an ordered record of a cellular event. We apply this approach to track the transition from a pluripotent state to a two-cell (2C)–like state in mouse embryonic stem cells (mESCs). The results provide compelling evidence for the transient nature of the 2C-like state. Additionally, our system shows consistent mutation rates across diverse cell types in a mouse gastruloid model, underscoring its robustness and versatility across various biological contexts. This technique not only improves our ability to study single-cell dynamics but also creates new opportunities for recording other temporal signals—in other words, using dynamic barcoding as a molecular clock in individual cells.

41 **INTRODUCTION**

42 Cellular behaviour is intrinsically dynamic, undergoing alterations in response to internal and
43 external stimuli. Different methodologies are commonly used to track or infer these changes.
44 However, these methods present several limitations. For example, methods based on live-cell
45 fluorescence microscopy are often incompatible with *in vivo* studies and are restricted in terms
46 of long-term and throughput capabilities (*1*). Other methods, such as those based on inference
47 algorithms using single-cell RNA sequencing (scRNA-seq) have low temporal resolution, as
48 scRNA-seq only captures a snapshot of gene expression at one specific time point (*2*, *3*).

49 DNA memory systems based on CRISPR technology have emerged as valuable tools for
50 recording dynamic events (*4–6*). These systems exploit CRISPR-based techniques to induce
51 permanent genetic modifications at precise genomic locations. By temporally regulating the
52 delivery of CRISPR components, these systems can generate DNA mutations that function as
53 molecular barcodes, enabling retrospective analysis of cellular activities. A variety of DNA
54 memory devices have been developed to track a wide range of biological signals (*4*), including
55 gene expression (*7*, *8*), chemical exposure (*8–10*), lineage of origin (*11–13*), clonality (*14*, *15*),
56 activation of signalling pathways (*16*) and inflammatory responses (*17*, *18*). Furthermore,
57 several methods now enable single-cell resolution readouts. These approaches typically
58 employ guide RNAs (gRNAs) targeting polyadenylation (polyA) sites, allowing simultaneous
59 sequencing of both single-cell transcriptomes and DNA barcodes (*19*, *20*). This integrated
60 strategy has been successfully applied to track lineage of origin in developmental (*21–27*) and
61 cancer studies (*28–30*). More recently, prime editing has also been applied to HEK293T cells
62 to track their lineage of origin at the single cell level *(15).*

63 Interestingly, dynamic CRISPR barcoding has also been proposed as a strategy for encoding
64 time (*18*). This approach relies on self-targeting gRNAs, a variant of the canonical form of

65 CRISPR-Cas9 gRNAs with the unique ability to repeatedly target their own sequence (*12*, *17*).
66 The continuous mutagenesis leads to a gradual accumulation of mutations over time, which
67 can be interpreted as a molecular record of elapsed time (*18*). However, since the target site is
68 the gRNA locus itself that lacks polyadenylation, this dynamic barcoding approach is not
69 compatible with standard single-cell RNA sequencing techniques.

70 In this study, we present scDynaBar, a novel method based on self-targeting gRNAs that
71 enables 25-day barcoding with high recovery efficiency for both genetic barcodes and
72 transcriptomes of individual cells using standard sequencing technologies. By coupling
73 barcoding with the expression of Zscan4c, we successfully demonstrate the versatility of
74 scDynaBar in tracking the transition from 2C-like states to pluripotency in mESCs *in vitro*.
75 This approach revealed that the 2C-like state is transient and does not persist over extended
76 periods. Additionally, our research shows consistent mutation rates in mouse gastruloids,
77 suggesting similar DNA repair rates among different cell types. These findings highlight the
78 broad potential of scDynaBar for tracking biological processes at single-cell resolution.

79

80 **RESULTS**

81 **Dynamic barcoding**

82 We aimed to develop a versatile system that can (i) record molecular events over extended
83 periods, and (ii) simultaneously profile genetic barcodes and gene expression at the single-cell
84 level, while being compatible with standard commercial sequencing technologies for easy
85 implementation. To achieve this, we engineered self-targeting gRNAs (*17*) so that they can be
86 retrieved from a polyadenylated transcript (expressed barcode). We also included an mCherry
87 reporter which enables easy visualization and selection of targeted cells (**Figure 1A**).

88 To investigate the dynamics of the system, and to test its ability to detect the barcodes at the
89 RNA level, we performed a time-course experiment using seven different gRNAs with varying
90 protospacer sizes (21 or 26 base pairs [bp]) and nucleotide compositions (**Supplementary**
91 **Figure 1**). We also aimed to evaluate the relative efficacies of barcoding using standard Cas9
92 and a base editing system, as the latter avoids inducing double-strand breaks. Specifically, we
93 used the BE3 base editor, which consists of a Cas9 nickase fused to the cytidine deaminase
94 APOBEC and the uracil DNA glycosylase inhibitor (UGI) domain (*32*). The UGI domain
95 facilitates uracil retention, ensuring precise C:G to T:A substitutions within a 4 to 8 nucleotide
96 window (*32*). In its absence, the frequency of indels increases, along with a higher incidence
97 of other substitutions (*32*, *33*). Therefore, to enhance mutational diversity in our approach, we
98 used a BE3 system lacking this domain (APOBEC–XTEN–dCas9(A840H)) (*32*). Both Cas9
99 constructs contained a constitutive promoter (CMV early enhancer fused to modified chicken
100 β-actin promoter) and a GFP reporter. Expression of the constructs was controlled by a Cre-
101 responsive FLEX switch, ensuring that expression occurred only after recombination. We co-
102 transfected individual gRNAs together with one of the two Cas9 constructs into mESCs. After
103 stable integration, we activated Cas9 by adding Cre recombinase to the culture media and then
104 collected cells from this mixed polyclonal population at various time points, up to day 18
105 (**Figure 1B**). We then selected cells positive for both reporters (GFP and mCherry) by
106 fluorescence-activated cell sorting (FACS) and subsequently performed bulk amplicon
107 sequencing on their RNA (see **Supplementary Figure 2 and Methods**) (**Figure 1B**).

108 To investigate the general dynamics of the systems, we first classified the barcode sequences
109 into three groups: (1) the original barcode, in which no editing occurred, (2) an active barcode,
110 in which editing occurred in the protospacer region but with the PAM sequence still uncut, and
111 (3) an inactive barcode, in which editing occurred in both the protospacer regions and the PAM
112 sequence, preventing further mutagenesis. Our data are consistent with sequential editing, as

they show increased level of active and inactive gRNAs, and a decreased frequency of original barcodes, over time (**Figure 1C**). The increased editing rate is consistent when using any of the seven gRNAs that we tested, as well as with either version of Cas9 (**Figure 1D**) (Jonckheere-Terpstra test; $p = 2 \times 10^{-13}$). Background editing in the absence of Cre (at day 0) was low (averaging 3% across experiments), likely resulting from spontaneous Cas9 expression (**Supplementary Figure 3**). After 18 days of editing, the system still contained barcodes with no mutations (mean original barcode frequency, 26.8%), indicating that mutagenesis could potentially be extended beyond this day (**Figure 1D**). We next assessed the

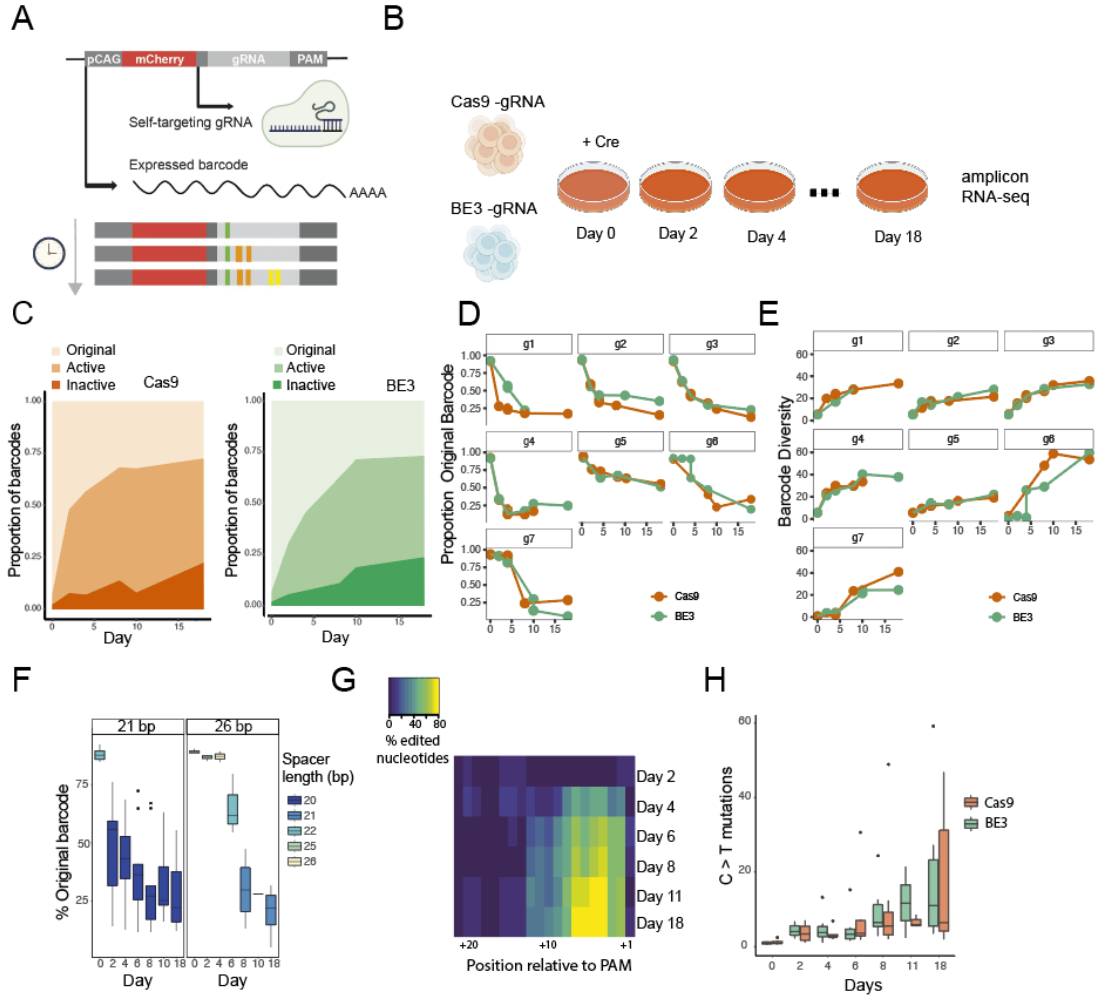

Figure 1. A. *Schematic representation of dynamic barcoding with a poly-A readout.* ***B.*** *Schematic representation of the experimental setup.* ***C.*** *Proportion of barcodes based on their mutational profiles for Cas9 (left) and BE3 (right). Barcodes are grouped into three categories: edits on the protospacer with intact PAM motif (active); absence of PAM motif (inactive); and uncut gRNA (original).* ***D.*** *Proportion of original barcodes over time across different gRNAs.* ***E.*** *Barcode diversity over time, considering mismatches, gaps and gap extensions across different gRNAs.* ***F.*** *Proportion of original barcodes over time for gRNAs with 21-bp spacers (left) or 26-bp spacers (right). Box plots are coloured by the mean spacer length at different time points (Cas9 system).* ***G.*** *Percentage of the original nucleotide over time, aligning the spacer relative to the PAM sequence (Cas9 system).* ***H.*** *Percentage of C>T mutations over time, considering all different gRNAs classified by Cas9 versions. For all boxplots, the boxes represent the interquartile range (IQR), with the horizontal line inside each box indicating the median.*

121 diversity of the edited reads by comparing their sequences to the original barcode. In this
122 analysis, we performed pairwise alignments for over 100,000 barcode sequences and calculated
123 a diversity score considering mismatches, gaps and gap extensions. Similarly, all seven gRNAs
124 demonstrated a sequential increase in diversity over the 18 days (Jonckheere-Terpstra test;
125 $p = 8 \times 10^{-16}$), providing strong evidence for continuous mutagenesis as well as for their
126 capacity to effectively record molecular events (**Figure 1E, Supplementary Figure 4**). In
127 agreement with previous studies, we also observed that in the Cas9 system 26-bp gRNAs
128 exhibit a slower editing rate compared to 21 -bp gRNA during the initial four days (**Figure 1F**)
129 (*31*) (Day 4, Mann-Whitney-Wilcoxon test; p = 0.0005). After this time point, the frequency
130 of intact barcodes for both the 21-bp and the 26-bp barcodes became very similar. This could
131 be attributed to the accumulation of deletions in the 26-bp gRNAs (**Figure 1F**), potentially
132 leading to an increased editing rate at later time points.

133 Next, we analysed the distribution of mutagenesis relative to the PAM of each gRNA in the
134 Cas9 system. As expected from the activity of Cas9, we observed a preferential accumulation
135 of mutations near the cut site, specifically within three nucleotides upstream of the PAM site
136 (**Figure 1G**). We then compared the specific types of edits in the BE3 system to the standard
137 Cas9. Notably, we observed a similar accumulation of indels over time in both systems (Mann-
138 Whitney-Wilcoxon test; p = 0.45, **Supplementary Figure 5**). This could be attributed to the
139 absence of the UGI domain, which may lead to DNA repair by alternative cellular mechanisms,
140 ultimately resulting in indel formation. Despite the lack of the UGI domain, our BE3 system
141 exhibited a slightly higher frequency of C>T mutations at most time points, with an average
142 difference of 6.9% (**Figure 1H**).

143 **Reproducibility and window of activity**

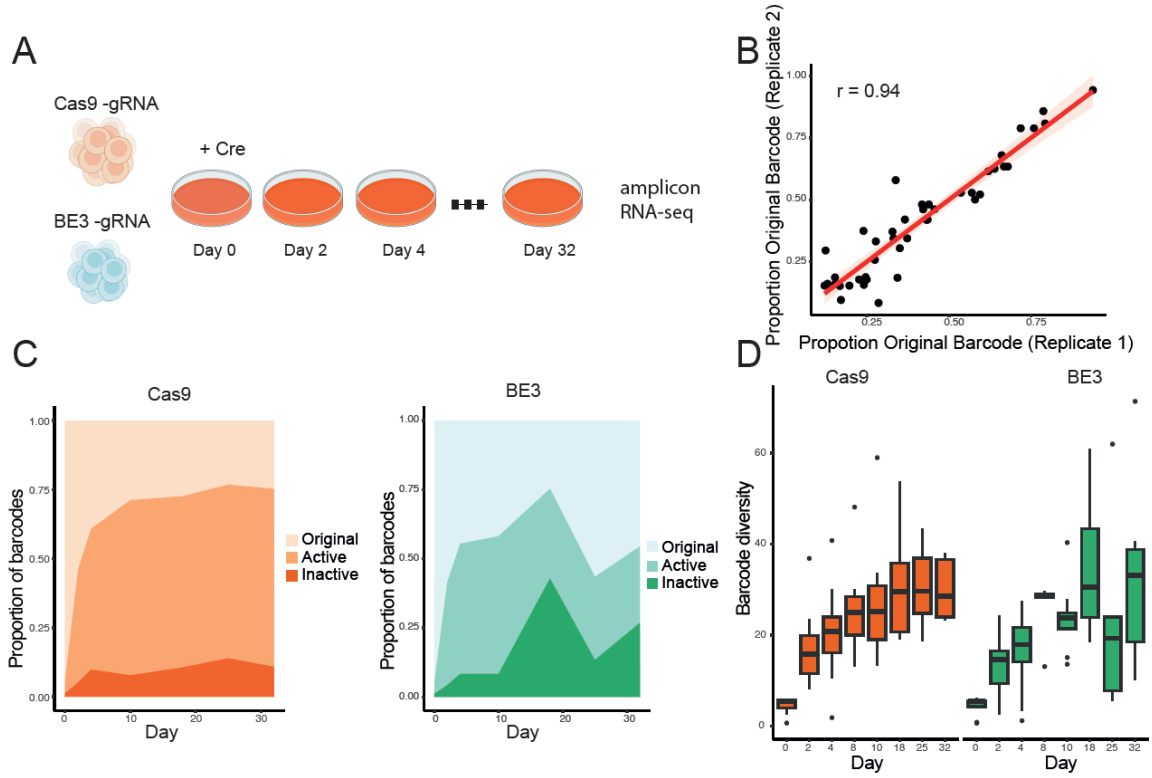

***Figure 2. A**. Schematic representation of the experimental setup. **B**. Pearson's correlation of original barcode frequencies between biological replicates from days 0 to 18. Each point represents the correlation coefficient between biological replicates considering gRNA, experiment type and time point. A total of 86 samples were analysed; including 50 samples from theCas9 experiment and 36 from the BE3 experiment. **C**. Proportion of barcodes based on their mutational profile: edits on the protospacer with intact PAM motif (active); lack of PAM motif (inactive); and uncut gRNA (original) according to Cas9 (left) or BE3 (right). **D.** Barcode diversity over time, considering mismatches, gaps and gap extensions, pooling all gRNA for Cas9 (left) and BE3 (right). In the boxplots, the boxes represent the IQR with the horizontal line inside each box indicating the median.*

We next aimed to extend the duration of mutagenesis to determine the maximum period during which the system can remain active and continue to generate mutations. As before, each of the seven gRNAs was individually co-transfected with one of the Cas9 constructs and then processed at various time points, up to day 32 (**Figure 2A**). We then compared original barcode frequencies across samples with two biological replicates (considering gRNA, day, and experiment, n=86). Remarkably, we observed consistent results between biological replicates for the initial 18 days, with a Pearson's correlation coefficient of 0.94 ($p < 2.2 \times 10^{-16}$), indicating the high reproducibility of our system (**Figure 2B**). These results also indicate that the Cas9 system remained active until day 25, albeit working at a slower rate (**Figure 2C, D**). In contrast, the BE3 system exhibited a significant increase in the frequency of original barcodes and a decrease in sequence diversity at day 25 (**Figure 2C, D**). We hypothesize that

155 this may result from differences in cellular fitness. Cells with high editing levels, particularly
156 those with mutations in the PAM sequence, may no longer target the gRNA locus, leading to
157 potential APOBEC-mediated off-target effects that could cause selective depletion (*34*). In
158 contrast, cells with an intact PAM sequence would continue to recruit APOBEC to the gRNA
159 locus, potentially reducing off-target effects and promoting their enrichment over time.
160 Nonetheless, future experiments are needed to better understand this phenomenon.

161 In conclusion, we demonstrate that both systems are effective for sequential barcoding, with
162 BE3 achieving comparable levels of barcode diversity in experiments conducted over a two-
163 week period and Cas9 being more suitable for long-term applications.

164 **Simultaneous detection of genetic barcodes in single cells**

165 We then evaluated whether genetic barcodes could be simultaneously recovered together with
166 transcriptomic data using standard single-cell RNA sequencing. First, based on our previous
167 observations, we selected gRNA g3 in combination with the canonical form of Cas9. We then
168 established a clonal cell line to minimize potential variability due to different integration sites
169 between individual cells. Using qPCR on genomic DNA, we determined that this clonal cell
170 line contains a single integration (**Methods**, **Supplementary Figure 6).** We grew these cells
171 under serum/LIF conditions and following Cre induction, we FACS-sorted double-positive
172 cells (for GFP and mCherry) on days 4 and 10 (**Figure 3A**). Additionally, we included a non-
173 induced group that showed minimal Cas9-GFP expression at day 10 (GFP = 0.1%), which
174 confirmed low levels of background activity.

175 Cells were processed using the 3' 10X Genomics platform, where they were encapsulated in
176 droplets with barcoded PolyT-coated beads and subjected to whole transcriptome amplification
177 following the standard 10x Genomics scRNA-seq 3′ protocol. We then specifically amplified

178 and sequenced the genetic barcodes from the cell-barcoded cDNA (**Figure 3A**). Overall, we
179 successfully recovered genetic barcodes from 97% of cells that passed transcriptome quality
180 control, demonstrating the efficiency of our approach for simultaneous transcriptome and
181 barcode detection.

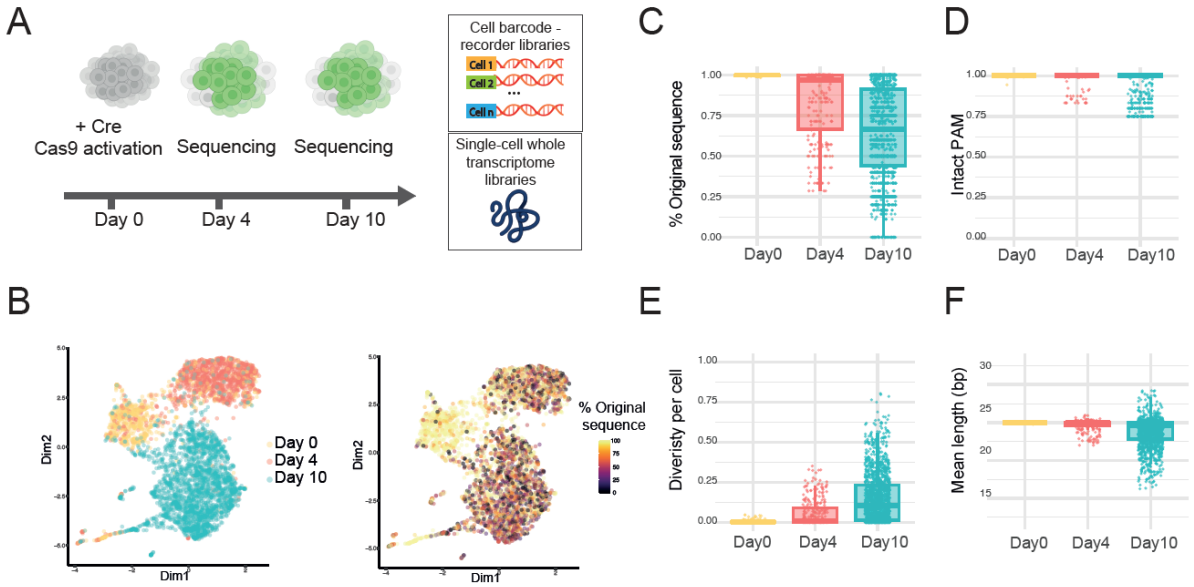

Figure 3 A. *Schematic representation of the experimental setup.* ***B.*** *t-SNE plot coloured by cluster: non-induced (day 0) and induced (day 4 or day 10) (left). Colour indicates the mean percentage of the original barcode sequence per cell (right).* ***C–F.*** *Boxplot of results at days 0, 4 and 10 showing* ***C.*** *the percentage of the original barcode sequences per cell;* ***D.*** *the mean proportion of barcodes with full PAM sequence per cell;* ***E.*** *mean sequence diversity per cell and* ***F.*** *mean length of the barcodes per cell. For all boxplots, the boxes represent the IQR, with the horizontal line inside each box indicating the median. Each dot represents an individual cell, with data points displayed within the 95% confidence interval.*

182 t-SNE analysis revealed three clusters of cells, corresponding to the different time points: non-
183 induced (day 0; $n = 495$), induced at day 4 ($n = 626$) and induced at day 10 ($n = 1117$) (**Figure**
184 **3B**). The most frequent barcodes sequences are listed in **Supplementary Table 1**, illustrating
185 the progressive increase in edited barcodes over time. For each cell, we assessed the level of
186 barcoding by analysing: the proportion of reads carrying the original barcode sequence, the
187 mean barcode diversity score (calculated as described previously), the average length of the
188 barcode sequence, and the percentage of barcodes carrying a PAM sequence (**Figure 3C–F**).
189 Our findings align with the results in bulk, showing sequential editing over time (Jonckheere-
190 Terpstra test; $p = 2 \times 10^{-04}$, 1000 permutations). We observed a decrease in the presence of
191 original sequences along with a decline of the proportion of barcodes carrying a PAM motif

192 (**Figure 3C, D**). Additionally, we observed an increase in barcode diversity and greater
193 variability in their lengths (**Figure 3E, F),** along with increased number of unique barcode
194 sequences per cell **(Supplementary Figure 7).** We also observed that the 1,480 edited gRNAs
195 sequences were unlikely to have off-targets effects that could affect cell viability
196 (**Supplementary Table 2**). Altogether, these data demonstrate the effectiveness of dynamic
197 barcoding in single cells and the capability of the method to simultaneously capture barcodes
198 and transcriptomic information using standard single-cell technologies.

199 **Recording dynamic transitions**

200 Having established the efficacy of scDynaBar in single cells, we next applied it to track
201 transitions between pluripotency and totipotency-like states. Under standard serum/LIF culture
202 conditions, a small population (less than 1%) of mESCs spontaneously emerges that exhibits
203 features resembling the totipotent 2C stage (*35*, *36*). These features include a specific
204 transcriptional profile, such as the expression of Zscan4 genes, increased histone mobility,
205 DNA demethylation and the capacity to contribute to both embryonic and extraembryonic
206 tissues (*35*, *37*, *38*). Although it is believed that the 2C-like state cannot self-propagate but
207 rather continuously undergoes transitions to a pluripotent state, these dynamics have not been
208 directly measured (*35*, *39*). To track 2C-like conversions, we integrated our barcoding
209 approach with a pZscan4-CreERT2 construct (**Figure 4A**) (*40*). With this setup, cells entering
210 the 2C-like state permanently activate the barcoding cassette during treatment with tamoxifen.
211 After establishing a monoclonal line, cells were treated with tamoxifen for 12 days. Following
212 treatment, we observed an increase in GFP-positive cells (9% tamoxifen-treated cells; 0.1% in
213 untreated cells). Double-positive cells (GFP- and mCherry-positive) were FACS-sorted and
214 processed for single-cell RNA-seq and barcoding sequencing (**Figure 4A**). We also sequenced
215 a portion of GFP-negative cells as a control.

216 After cell and barcode quality control, we recovered 3,352 GFP-positive cells and 1,270 Cas9-
217 GFP-negative cells (barcode recovery rate = 98%). t-SNE analysis identified three clusters
218 corresponding to Cas9-GFP-negative cells and two clusters representing Cas9-GFP-positive
219 cells. Within the Cas9-GFP-positive population, we observed variable levels of barcode
220 diversity, indicating the activation of barcoding at distinct time points during our time course
221 (**Figure 4B**). t-SNE analysis also revealed a cluster of 24 cells corresponding to 2C-like cells,
222 characterized by expression of totipotency markers, such as Zscan4c (**Figure 4B and 4C).**

223 Cells in the pluripotent state, characterized by a lack of Zscan4c expression, exhibited high
224 variability in their barcode diversity (**Figure 4B**) (Diversity Brown-Forsythe Test; $p = 0.01$;
225 Original barcode sequence Brown-Forsythe Test; $p = 0.0006$). This high variability indicates
226 that the CRISPR barcoding system was activated early upon entry into the 2C-like state, at
227 different time points in each of the cells. As a result, the continuous activity of the barcoding
228 system led to an accumulation of different levels of diversity over time. In contrast, all cells in
229 the 2C-like state (i.e., with Zscan4c expression) displayed low barcode diversity, along with a
230 high proportion of the original barcode sequence (**Figure 4D**) (Diversity Mann-Whitney-
231 Wilcoxon test; $p = 0.0007$; Original barcode sequence Mann-Whitney-Wilcoxon test; $p =$
232 0.0004). This low diversity cannot be attributed to reduced coverage of the barcode cassette in
233 this population (**Supplementary Figure 8**). The absence of 2C-like cells with high barcode
234 diversity indicates that they transitioned into this state only recently. These findings prove the
235 prevailing hypothesis in the field that ESCs undergo continuous dynamic transitions into and
236 out of the 2C-like state, a phenomenon that has been difficult to measure directly until now
237 (*35*, *39*, *41*). Our results also indicate that the 2C-like cells that became pluripotent did not re-
238 enter into the 2C-like state during the experiment. This could be attributed to a combination of
239 factors: probability, as only about 1% of the cells are in the 2C-like state at any given time, and
240 potential inhibitory or promoting signals that might regulate re-entry into this state.

To identify candidate genes that may regulate these transitions, we performed a correlation analysis between the transcriptome profiles and diversity scores in pluripotent cells. Notably, Dppa4, a gene implicated in the 2C-like state emerged as one of the top correlated genes. (**Supplementary Table 3, Supplementary Figure 9**). These findings suggest that the progressive upregulation of Dppa4 in pluripotent cells may facilitate the transition toward the 2C-like state. Indeed, previous studies have demonstrated that Dppa4 depletion inhibits the 2C-like reprogramming in mESCs (*42*, *43*). Other genes correlated with the diversity score potentially involved in the 2C-like transition include the Jumonji Domain Containing 8 (*JMJD8*) or Zinc Finger Protein 226 (*ZNF226)* **(Supplementary Figure 9).**

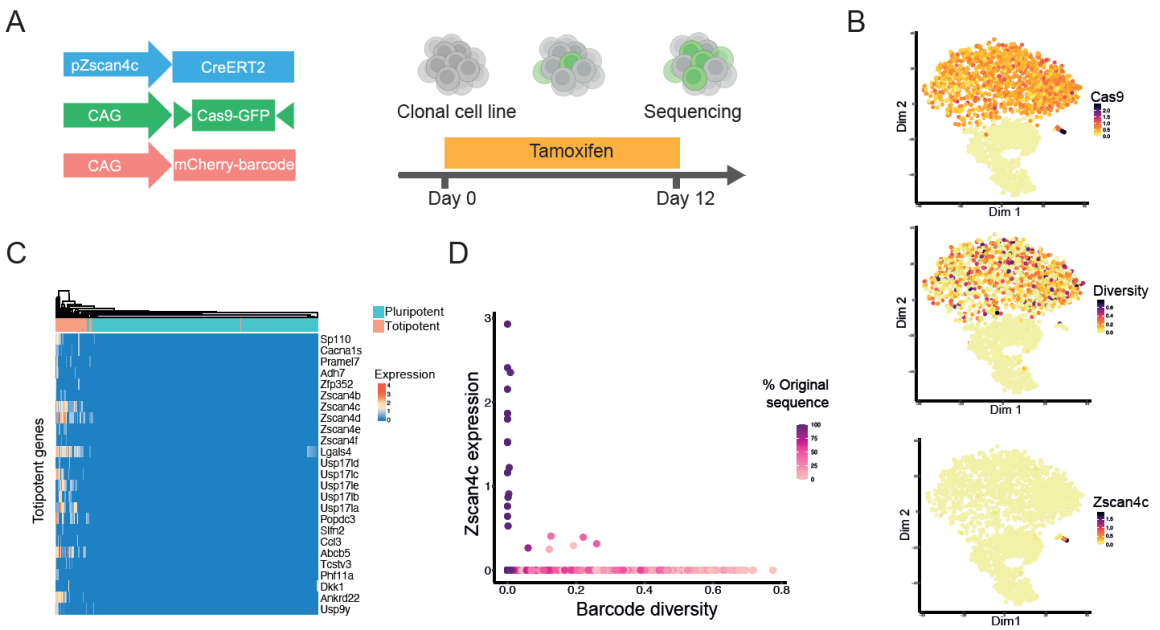

Figure 4. A. *Schematic representation of the experimental setup for tracking 2C-like state transitions.* ***B.*** *t-SNE plot coloured by (top) Cas9 expression, (middle) mean barcode diversity per cell, and (bottom) Zscan4c expression (log2 normalised counts).* ***C.*** *Heatmap displaying gene expression (log2 normalised) for top markers for the totipotent cluster.* ***D.*** *Scatterplot displaying Zscan4c expression (log2 normalised) (y-axis) against barcode diversity (x-axis) per cell, with colour indicating the percentage of original barcode sequences.*

These results demonstrate the effectiveness of scDynaBar in capturing the dynamic transitions between these states, making it a versatile tool for studying complex cellular dynamics that could not be previously tracked.

Dynamic barcoding in mouse gastruloids

254 To investigate the mutation rate across diverse cell types, we applied scDynaBar to mouse
255 gastruloids, which are three-dimensional structures that mimic early developmental processes
256 and comprise a diverse array of cell types (*44*). For this, we used our previously established
257 mESC monoclonal cell line (**Figure 3**). Two days after Cre induction, mESCs were seeded for
258 aggregation and subsequent gastruloid formation (*44*) (**Figure 5A**). Six days after induction,
259 Day 4 gastruloids were dissociated, and the cells were processed for single-cell RNA and
260 barcode sequencing. These gastruloids exhibited normal morphology and low levels of cell
261 death (**Supplementary Figure 10**). After the cell and barcode quality controls, we recovered
262 1,057 Cas9-GFP-positive cells (i.e., GFP counts >1) and assigned cell types by mapping RNA
263 expression profiles to a reference atlas of mouse embryos, from E6.5 to E8.5 (*45*) (**Figure 5B**).
264 This analysis revealed a bias towards the mesodermal lineage, consistent with our previous
265 studies showing that gastruloids often favour mesodermal or ectodermal cell types (*46*). We
266 then computed the proportion of the original barcode sequence and the barcode diversity score
267 for each cell and found no clear differences between cell populations (**Figure 5C,**
268 **Supplementary Figure 11A**), indicating that the barcoding rate is similar across diverse cell
269 types (Kruskal-Wallis Test; $p = 0.3557$).

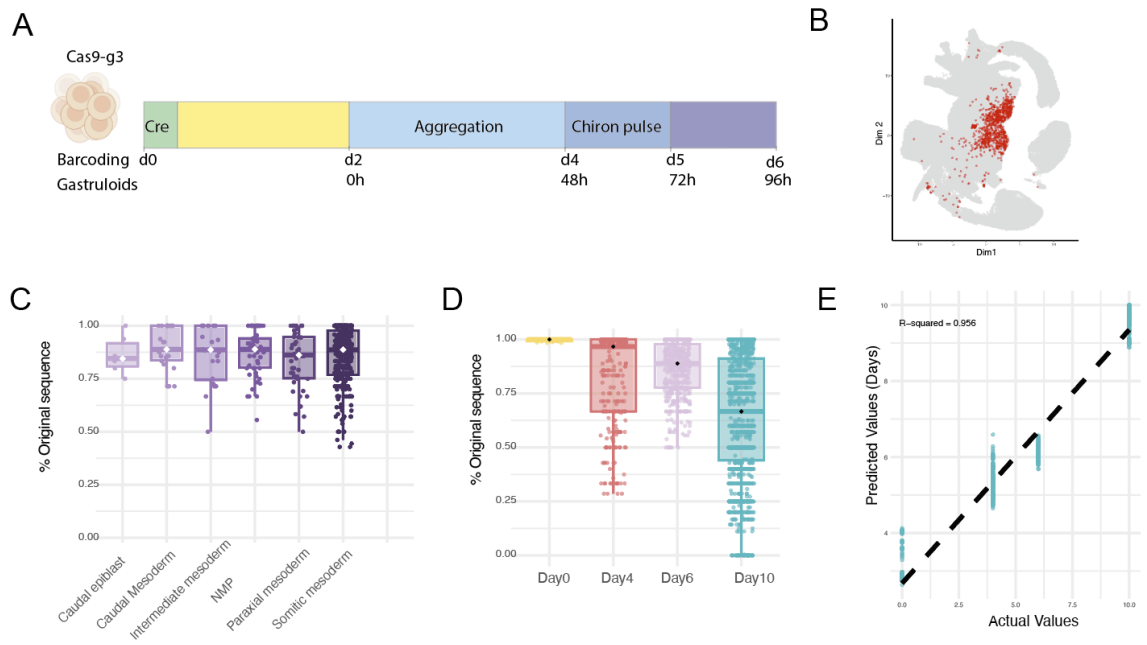

***Figure 5. A**. Schematic of the experimental design for gastruloid formation and barcoding. Cre induction was performed on day 0 (d0). After two days (yellow bar), cells were plated for aggregation (light blue). On day 4 (d4), a Chiron pulse (CHIR99021) was applied to promote gastruloid elongation and cell differentiation (dark blue). Gastruloids were then further cultured (purple bar) and collected on day 6 (d6) for single-cell sequencing **B**. UMAP projection showing developmental stages from a reference atlas of mouse embryos between E6.5 and E8.5, with extra-embryonic cells excluded. Gastruloid cells are highlighted in red. Nearest neighbour analysis was used to assign cell-type labels to the gastruloid cells based on their proximity to the cells in the reference atlas. **C**. Boxplot showing the percentage of the original barcode sequence was calculated for each cell grouped by cell type. **D**. Boxplot showing the distribution of the proportion of original barcodes across different time points in single cells. **E**. Scatter plot showing predicted (y) versus actual (x) time points (days) using a random forest model, with R-squared values of 95% for test data. For all boxplots, the boxes represent the IQR with the horizontal line inside each box indicating the median.*

Comparing these data with our previous single cell dataset (**Figure 3**), we observed that gastruloids collected at day 6 exhibited levels of barcoding that ranged between those observed at day 4 and day 10 (**Figure 5D, Supplementary Figure 11B).** Specifically, the median value of the original barcode sequencing was 85% at day 6, compared to 96% at day 4 and 66% at day 10, indicating an accumulative increase of mutations over time (Jonckheere-Terpstra test; $p = 2 \times 10^{-04}$; 1000 permutations) (**Figure 5D**). We hypothesized that the gradual increase in barcode editing could be used to determine the duration of barcode activity in single cells. To test this hypothesis, we developed a temporal predictor using random forest regression on our single cell datasets (days 0, 4, 6 and 10). The predictor was trained on 80% of the data, incorporating barcode features as variables (mean barcode length, percentage of original sequences, diversity mean and coverage). Using this predictor, we achieved an R^2 of 98% on

281 the training set, and of 95% on the test data (**Figure 5E**). Achieving this high level of accuracy
282 despite using a limited number of time points suggests that DNA barcodes can effectively be
283 used to predict the duration of barcoding and record the duration of an event in single cells.
284 This highlights the strong potential of dynamic barcoding to function as a molecular clock for
285 time tracking in different cellular contexts.

286 **DISCUSSION**

287 In this study, we introduce scDynaBar, a novel approach for dynamic cellular barcoding in
288 single cells. We achieved this by engineering self-targeting gRNAs (*31*), enabling the
289 simultaneous capture of both genetic barcodes and the transcriptomes of individual cells. This
290 method requires minimal adjustments to existing commercial single-cell sequencing
291 workflows offering a high level of both versatility and ease of scalability.

292 We demonstrated that dynamic barcoding leads to the sequential accumulation of genetic
293 diversity over 25 days through continuous targeting, with high reproducibility. This represents
294 a substantial advancement as compared to other single-cell barcoding methods, in which
295 mutations typically occur within the first 48 h (*22*, *26*). The accumulation of mutations over
296 time can be assessed through multiple measures, including i) a reduction in the proportion of
297 original sequences, ii) a decrease in the frequency of sequences with an intact PAM motif and
298 iii) a notable increase in both the diversity of spacer sequences and iv) the variability of their
299 lengths. Interestingly, we observed comparable rates of mutagenesis and barcode diversity
300 using standard Cas9 or the modified cytosine base editor BE3 (*32*), which fuses APOBEC with
301 nCas9. Although potential adverse effects of BE3 were observed during prolonged barcoding,
302 which require further investigation, its efficacy was demonstrated within a 2-week period. This
303 system could be particularly valuable for applications that are incompatible with the generation
304 of double-strand DNA breaks.

305 As a proof of concept for scDynaBar's potential applications, we demonstrated its ability to
306 record dynamic cell transitions. By collecting data at a single endpoint and using a CreERT2
307 protein controlled by the Zscan4c promoter, we documented the transition of mESCs from the
308 pluripotent state to the 2C-like state. In this experimental setup, the diversity of barcodes
309 encodes the timing of the cell transitions to the 2C-like state. Our findings showed that all 2C-
310 like cells had recently transitioned to this state, as evidenced by a lack of mutations in their
311 barcodes. These results underscore the transient nature of the 2C-like state and support the
312 current hypothesis suggesting that the 2C-like state cannot self-perpetuate (*35*, *39*, *41*).
313 Additionally, these findings illustrate the potential of our approach for studying complex
314 cellular dynamics that are currently difficult to track with existing methodologies.

315 Our observations from a mouse gastruloid model revealed normal phenotypes, indicating the
316 preservation of differentiation potential in cells with active barcoding. Additionally, we
317 observed consistent DNA repair rates across different cell types, underscoring the robustness
318 of scDynaBar and its potential for application in a wide range of biological contexts.
319 Nonetheless, further experiments are required to better understand how factors such as
320 variations in Cas9 levels, DNA repair kinetics, and DNA context influence barcode diversity.

321 Finally, we believe scDynaBar is highly adaptable and easy to implement, making it suitable
322 for recording a wide variety of temporal events in single cells. For example, by modulating
323 Cas9 activity, scDynaBar could be tailored to track the duration of a specific event, such as the
324 activity of a transcription factor or the response to external stimuli. This flexibility opens new
325 opportunities for capturing dynamic cellular signals and processes at the single-cell level.

326

327 **MATERIAL AND METHODS**

328 **Vector construction**

329 The barcoding cassette used in this study were constructed by incorporating gBlock (IDT
330 DNA) synthesized DNA fragments, including CAG promoter, mCherry, and scaffold, into a
331 piggyBac backbone. Different gRNAs (spacers), obtained from Sigma-Aldrich, were cloned
332 into this vector. The sequences of these spacers are provided in the **Supplementary Figure 1**.
333 The Cas9-2A-GFP vector used in this study is based on Cong et al. (2013) (*47*) and was cloned
334 into a piggyBac backbone with a one-way genetic switch (FLEX) system. The BE3 system,
335 kindly provided by Alexis Komor (*32*), was further modified by removing the uracil
336 glycosylase inhibitor (UGI) and then incorporating it into a piggyBac backbone as nCas9-
337 rAPOBEC1-2A-GFP in a one-way genetic switch (FLEX) system.

338 The plasmid carrying CreERT2 under the control of the Zscan4c promoter (pZscan4-CreERT2
339 cells), as described in Zalzman et al. (2010) (*40*), was generated by VectorBuilder with a
340 puromycin resistance marker.

341 **Mouse embryonic stem cell culture**

342 E14 mESCs were cultured under standard serum/LIF conditions in DMEM (Gibco, 11995-
343 040) supplemented with 15% fetal bovine serum, 1 U/ml penicillin and 1 mg/ml streptomycin
344 (Gibco, 15140-122), 0.1 mM nonessential amino acids (Gibco, 11140-050), 4 mM GlutaMAX
345 (Gibco, 35050-061), 50 μM β-mercaptoethanol (Gibco, 31350-010) and 103 U/ml LIF (Stem
346 Cell Institute, Cambridge). Cells were maintained at 37°C in a 5% CO_2 atmosphere on
347 gelatinized tissue-culture plates. Media was changed daily, and cells were passaged every other
348 day using trypsin-EDTA (Thermo Fisher Scientific, 25200056).

349 Stable cell lines were generated through transfection using Fugene (Promega, E2311), followed
350 by drug selection and fluorescence-activated cell (FAC) sorting. Clonal cell lines were isolated
351 through additional rounds of subcloning.

352 To determine the number of copies of the barcode construct integrated in the clonal cell line
353 used in Figure 3 and Figure 5, a genomic qPCR was performed. Genomic DNA was extracted
354 from wild-type (wt) mESCs and from the clonal cell line, using the DNeasy Blood and Tissue
355 Extraction Kit (Qiagen). The qPCR was performed using the Brilliant III Ultra-Fast SYBR®
356 Green QPCR Master Mix in a Roche LightCycler® 480 Instrument II following Agilent
357 Technologies®' guidelines of one 3-minute cycle at 95ºC and 40 cycles of 5 seconds at 95ºC
358 and 10 seconds at 60ºC with the primers below. Samples were tested in triplicates and a
359 negative control with water was included for each primer combination. Three different DNA
360 amounts were tested: 5 ng, 10 ng and 20 ng. For quantification, the $2^{-\Delta Ct}$ method was used,
361 using GAPDH as a reference for the relative quantification of both 2n DNA amplicons
362 (ACTB1, ACTB2 and Intergenic) and the integrated barcoding cassette (Barcode 1 and
363 Barcode 2).

Primer	**Sequence**	**Amplicon Size (bp)**
GAPDH mouse Fw	AACAATCTCCACTTTGCCACTGC	100
GAPDH mouse Rv	GTTCTGATCTCAGCTCCCCTGTTT	
ACTB mouse 1 Fw	GGCCTCGTCACCCACATAGGA	92
ACTB mouse 1 Rv	GGGATCGATGCCGGTGCTAAGA	
ACTB mouse 2 Fw	CCAGAGGCATACAGGGACAG	133
ACTB mouse 2 Rv	GCCCTGAGTGTTTCTTGTGG	
Intergenic Fw	TGCAAACAGCTGACCTCCAA	104

Intergenic Rv	GTCCTGGGTTAGACGCTTCC	
Barcode 1 Fw	CAATGCCCTGGCTCACAAAT	95
Barcode 1 Rv	AGCCAGAAGTCAGATGCTCA	
Barcode 2 Fw	GAAGGACGGCGGCCACTA	92
Barcode 2 Rv	TGATGTCGACGTTGTAGGCG	

364

365 Cas9 induction was carried out using Cre recombinase (Takara, 631449) in media
366 supplemented with 6 µg/mL polybrene (Sigma, H9268), according to the manufacturer's
367 instructions. pZscan4c-CreERT2 cells were treated with 4-hydroxytamoxifen (1 µM) for 12
368 days (Sigma, H7904).

369 **Gastruloid culture**

370 The mESC clonal cell line containing the barcoding system was cultured under standard
371 serum/LIF conditions. Induction was carried out as before using Cre recombinase (Takara,
372 631449) in media supplemented with 6 µg/mL polybrene (Sigma, H9268), according to the
373 manufacturer's instructions. After two days, cells were prepared for gastruloid formation using
374 a previously described protocol (*44*). Specifically, mESCs were dissociated into single cells
375 with trypsin-EDTA (Thermo Fisher Scientific, 25300096). Cells were then washed twice with
376 pre-warmed PBS (Thermo Fisher Scientific, 14190144), and the pelleted cells were then
377 resuspended in 5 ml of N2B27 medium of a 1:1 mix of DMEM/F12 (Thermo Fisher Scientific,
378 11320033) and Neurobasal (Thermo Fisher Scientific, 21103049), supplemented with 0.5× N-
379 2 Supplement (Cell Therapy Systems, A1370701), 0.5× B-27 Supplement (Thermo Fisher
380 Scientific, 17504044), 2 mM GlutaMAX, 10 U/ml penicillin-streptomycin and 0.1 mM 2-

381 mercaptoethanol. Cells were then diluted to a density of 7500 cells/ml in N2B27 medium, and
382 40 µl of this dilution was added to each well of a U-bottom 96-well suspension culture plate
383 (Greiner Bio-One, 650185) to reach a density of 300 cells per well. The cells were left to
384 aggregate for 48 h. After this period, 150 µl of N2B27 medium containing 3 µM CHIR99021
385 (Department of Biochemistry, University of Cambridge) was added. Every 24 h, 150 µl of the
386 medium was replaced with fresh N2B27 medium without CHIR99021. On day 4, gastruloids
387 were harvested for sequencing: they were transferred to an Eppendorf tube, rinsed with PBS,
388 and dissociated into single cells using Accutase (StemPro, A1110501). Cells were then washed
389 twice with 5 ml of PBS containing 0.04% BSA (Gibco, 15260037) to remove the Accutase,
390 followed by filtration through a 50 µm strainer (Sysmex, 1050553). The cell count and viability
391 were determined using the Countess II Automated Cell Counter prior to single-cell sequencing.

392 **Bulk barcode sequencing**

393 Bulk barcode sequencing was performed on a mixed, non-clonal population. After stable
394 integration and induction, cells were sorted at various time points using either the BD Aria III
395 or the BD Influx High-Speed Cell Sorter. About 8K to 12K cells positive for GFP and mCherry
396 were collected for each sample. RNA was then extracted using the RNeasy Micro Kit (Qiagen,
397 74004). To amplify the gRNA loci, reverse transcription was performed as previously
398 described (*48*), with 1 µl of primer (GTGACTGGAGTTCAGACGTGTGCTCTTCCGATCT-
399 T(30)) and 500 ng of RNA. cDNA was amplified in a 20 µl reaction using KAPA HiFi HotStart
400 ReadyMix (KAPA Biosystems, KK2502) with the following primers:

401 Forward: 5′-
402 ACACTCTTTCCCTACACGACGCTCTTCCGATCT(N/NN/NNN)TCTTGTGGAAAGGA
403 CGAAACAC-3′

404 Reverse: 5′-
405 CAAGCAGAAGACGGCATACGAGATXXXXXXGTGACTGGAGTTCAGACGTGTGCT
406 CTTCCGATCT-3′

407 XXXXXX- index;

408 Random nucleotides (NNN, NN and N) were added to introduce sequence diversity, enhancing
409 variability over the constant sequence for sequencing purposes. The DNA product was then
410 purified with a 0.8:1 volumetric ratio of AMPure XP Beads (Beckman Coulter, A63881) and
411 the whole volume was resuspended in 20ul of PCR mastermix (KAPA HiFi Readymix) using
412 the primers:

413 Forward: 5′-
414 AATGATACGGCGACCACCGAGATCTACACTCTTTCCCTACACGACGCTCTTCCGA
415 TCT-3′

416 Reverse: 5′-CAAGCAGAAGACGGCATACGAGAT-3′

417 PCR products were purified using a 0.8:1 volumetric ratio of AMPure XP Beads, pooled, and
418 sequenced on a single end Illumina MiSeq run with 58 cycles (58 bp amplicon length) and an
419 8-cycle index.

420 **Single-cell sequencing**

421 A single-cell suspension was loaded into the 10X Chromium device, and libraries were
422 prepared using the 10X Single-Cell 3′ Library & Gel Bead Kit v2 (10X Genomics, PN-
423 120237), following the manufacturer's instructions. The following samples were each loaded

424 into a lane of the 10X Chromium Control chip: day 4, day 10, pZscan4c-CreERT2 cells,
425 gastruloids 1, gastruloids 2, and gastruloids 3.

426 Amplicon gRNA PCRs (KAPA HiFi Readymix) were performed for each of the 10X cDNA
427 samples using 1 µl of the cDNA and the following primers:

428 Forward: 5′-
429 ACACTCTTTCCCTACACGACGCTCTTCCGATCT(N/NN/NNN)TCTTGTGGAAAGGA
430 CGAAACAC-3′

431 Reverse: 5′-
432 AATGATACGGCGACCACCGAGATCTACACTCTTTCCCTACACGACGCTCTTCCGA
433 TCT-3′

434 As before, random nucleotides (NNN, NN and N) were added to introduce sequence diversity,
435 enhancing variability over the constant sequence for sequencing purposes. PCR products were
436 purified using a 0.8:1 volumetric ratio of AMPure XP Beads, and the whole volume was loaded
437 into a second nested PCR (KAPA HiFi Readymix) with the following primers:

438 Forward: 5′-
439 CAAGCAGAAGACGGCATACGAGATXXXXXXXXGTGACTGGAGTTCAGACGTGT
440 GCTCTTCCGATCT-3′

441 Reverse: 5′-
442 AATGATACGGCGACCACCGAGATCTACACTCTTTCCCTACACGACGCTCTTCCGA
443 TCT-3′

444 XXXXXX- index

445 After purification using AMPure XP beads, the enriched gRNA libraries were sequenced
446 together with the transcriptome libraries on the Illumina NovaSeq platform.

447 **Bulk barcode analysis**

448 A total of 160 samples were processed for bulk barcoding (see **Supplementary Table 4**). After
449 sample demultiplexing, reads that did not contain both the flanking regions on the U6 promoter
450 and the spacer regions on either side of the cassette were discarded ("AACAC" and
451 "TTAGAG" respectively). Barcodes with mean Illumina Phred scores below 28 were also
452 removed. Additionally, samples with fewer than 200 reads were excluded. After this quality
453 control, a total of 151 samples were processed for further analysis.

454 The percentage of original sequences was determined by comparing the spacer regions to the
455 original spacer sequences. To assess diversity, each barcode was aligned to the reference spacer
456 using the *pairwiseAlignment* function from the Biostrings R package (*49*). The alignment was
457 performed using a global-local approach with a substitution matrix that assigned a score of –1
458 for mismatches and +2 for matches, and a gap opening and extension penalties set to 5. The
459 diversity score for each sample was calculated as the average alignment score across its
460 individual barcodes. Finally, diversity scores were normalized across all samples to ensure
461 comparability. Aligned sequences were further analysed to compute nucleotide frequencies per
462 position.

463 **Single-cell transcriptome quality control and processing**

464 All 10X scRNA-seq data were processed using the 10X Genomics Cell Ranger pipeline with
465 the mm10 genome build, including the GFP sequence. For quality control, cells were discarded
466 if they had fewer than 3,000 detected genes and/or more than 7.5% of UMI reads originating
467 from mitochondrial genes (**Supplementary Figure 12**). Raw counts for each cell were

468 normalized by dividing the counts by their size factors, and the resulting log-normalized counts
469 were used for further analysis.

470 Broad clustering analysis and t-distributed stochastic neighbour embedding (t-SNE) plot
471 generation were performed using Seurat. Linear dimensional reduction was executed via
472 principal component analysis (PCA) using the Seurat function RunPCA, with highly variable
473 genes identified by the Seurat function FindVariableGenes as inputs. Fifteen principal
474 components were utilized to generate clusters and t-SNE plots using the Louvain algorithm
475 implemented in the Seurat function FindClusters.

476 **Gastruloid cell type assignment**

477 Cell types were assigned by aligning RNA expression profiles to a reference atlas as previously
478 described (*46*, *50*). Briefly, count matrices from both datasets were combined and normalized.
479 Highly variable genes were identified and used for PCA. Batch correction was performed to
480 eliminate technical differences between the query and atlas cells. Using the integrated data, a
481 k-nearest neighbours (kNN) graph was constructed. Each query cell's type was assigned by
482 determining the most common cell type among the 30 nearest neighbours in the atlas, using a
483 Dirichlet distribution for majority voting.

484 **Single-cell barcode library processing**

485 Fastq single-cell barcode libraries were processed to match cell IDs from the scRNA-seq
486 transcriptomes. Reads lacking the specified flanking regions on the U6 promoter and spacer
487 regions ("AACAC" and "TTAGAG" respectively) or those with an Illumina Phred score of
488 <28, were discarded (**Supplementary Figure 12**). Furthermore, for each UMI with at least
489 three barcode reads, a consensus barcode sequence was determined by selecting the sequence
490 present in over 50% of the retained UMIs. Diversity scores were calculated as in bulk analysis

491 by performing a pairwise alignment of each barcode with the gRNA spacer, using the
492 pairwiseAlignment function from the Biostrings package (*49*). The diversity score for each cell
493 was calculated as the average alignment score across its individual barcodes. Finally, diversity
494 scores were normalized across all cells to ensure comparability.

495 **Random forest model**

496 The random forest model was employed to evaluate whether barcode editing over time could
497 predict barcode duration in single cells. Single-cell datasets were used from days 0, 4, 6 and
498 10, whereby the mean barcode length, percentage of original sequences, mean diversity and
499 coverage were incorporated as features. For each dataset, 20% of the data was set aside for
500 testing, while the remaining 80% was used for training. The randomForest function from the
501 randomForest package (version *4.7-1.1*) was used to fit a regression model (*51*), with "day" as
502 the response variable and the selected features as predictors. Model performance was assessed
503 by predicting day values for both the training and test sets, and the R^2 statistic was calculated
504 to quantify the proportion of variance explained by the model.

505

506 **DATA AVAILABILITY**

507 Sequencing data have been deposited in the Gene Expression Omnibus (GEO) database under
508 the accession numbers GSE280613 and GSE280614 (token for revisions are: axavckacjfgzbez
509 and inqlyiuilbgbtqv). The scripts, processed data and metadata are accessible on the GitHub
510 repository: https://github.com/socyol/scDynaBar.git.

511

512 **COMPETING INTERESTS**

WR is a consultant and shareholder of Biomodal. AS, IK, CT, SC & WR are employees of Altos Labs. CAC is an employee of GSK.

REFERENCES

1. M. Maška *et al.*, *Nat. Methods*. **20**, 1010–1020 (2023).
2. G. La Manno *et al.*, *Nature*. **560**, 494–498 (2018).
3. L. Haghverdi, M. Büttner, F. A. Wolf, F. Buettner, F. J. Theis, *Nat. Methods*. **13**, 845–848 (2016).
4. R. U. Sheth, H. H. Wang, *Nat. Rev. Genet.* **19**, 718–732 (2018).
5. A. Pickar-Oliver, C. A. Gersbach, *Nat. Rev. Mol. cell Biol.* **20**, 490–507 (2019).
6. Y. Li, S. Li, J. Wang, G. Liu, *Trends Biotechnol.* **37**, 730–743 (2019).
7. S. Bhattarai-Kline *et al.*, *Nature*. **608**, 217–225 (2022).
8. F. Schmidt, M. Y. Cherepkova, R. J. Platt, *Nature*. **562**, 380–385 (2018).
9. F. Farzadfard, T. K. Lu, *Science (80-.).* **361**, 870–875 (2018).
10. R. U. Sheth, S. S. Yim, F. L. Wu, H. H. Wang, *Science (80-.).* **358**, 1457–1461 (2017).
11. A. McKenna *et al.*, *Science (80-.).* **353**, aaf7907–aaf7907 (2016).
12. R. Kalhor *et al.*, *Science (80-.).* **361** (2018), doi:10.1126/science.aat9804.
13. T. B. Loveless *et al.*, *Nat. Chem. Biol.* **17**, 739–747 (2021).

532 14. W. Zhang *et al.*, *Cell*. **184**, 2471–2486 (2021).

533 15. J. Choi *et al.*, *Nature*. **608**, 98–107 (2022).

534 16. W. Tang, D. R. Liu, *Science (80-.).* **360**, eaap8992 (2018).

535 17. S. D. Perli, C. H. Cui, T. K. Lu, *Science (80-.).* **353**, aag0511 (2016).

536 18. J. Park *et al.*, *Cell*. **184**, 1047–1063 (2021).

537 19. D. E. Wagner, A. M. Klein, *Nat. Rev. Genet.* **21**, 410–427 (2020).

538 20. A. McKenna, J. A. Gagnon, *Development*. **146**, dev169730 (2019).

539 21. A. Alemany, M. Florescu, C. S. Baron, J. Peterson-Maduro, A. Van Oudenaarden,
540 *Nature*. **556**, 108–112 (2018).

541 22. B. Spanjaard *et al.*, *Nat. Biotechnol.* **36**, 469–473 (2018).

542 23. B. Raj *et al.*, *Nat. Biotechnol.* **36**, 442–450 (2018).

543 24. M. M. Chan *et al.*, *Nature*. **570**, 77–82 (2019).

544 25. L. Li *et al.*, *Cell*. **186**, 5183–5199 (2023).

545 26. S. Bowling *et al.*, *Cell*. **181** (2020), doi:10.1016/j.cell.2020.04.048.

546 27. K. L. Frieda *et al.*, *Nature*. **541**, 107–111 (2017).

547 28. D. Yang *et al.*, *Cell*. **185**, 1905–1923 (2022).

548 29. J. J. Quinn *et al.*, *Science (80-.).* **371**, eabc1944 (2021).

549 30. K. P. Simeonov *et al.*, *Cancer Cell*. **39**, 1150–1162 (2021).

550 31. R. Kalhor, P. Mali, G. M. Church, *Nat. Methods*. **14**, 195–200 (2017).

551 32. A. C. Komor, Y. B. Kim, M. S. Packer, J. A. Zuris, D. R. Liu, *Nature*. **533**, 420–424
552 (2016).

553 33. L. Wang *et al.*, *Cell Res.* **27**, 1289–1292 (2017).

554 34. E. Zuo *et al.*, *Science (80-.).* **364**, 289–292 (2019).

555 35. T. S. Macfarlan *et al.*, *Nature*. **487**, 57–63 (2012).

556 36. M. Li, J. C. Izpisua Belmonte, *Nat. Cell Biol.* **20**, 382–392 (2018).

557 37. A. Bošković *et al.*, *Genes Dev.* **28**, 1042–1047 (2014).

558 38. M. A. Eckersley-Maslin *et al.*, *Cell Rep.* **17**, 179–192 (2016).

559 39. D. Rodriguez-Terrones *et al.*, *Nat. Genet.* **50**, 106–119 (2018).

560 40. M. Zalzman *et al.*, *Nature*. **464**, 858–863 (2010).

561 41. X. Fu, M. N. Djekidel, Y. Zhang, A transcriptional roadmap for 2C-like-to-pluripotent
562 state transition. Sci. Adv. 6, eaay5181 (2020).

563 42. A. De Iaco, A. Coudray, J. Duc, D. Trono, *EMBO Rep.* **20**, e47382 (2019).

564 43. M. Eckersley-Maslin *et al.*, *Genes Dev.* **33**, 194–208 (2019).

565 44. L. Beccari *et al.*, *Nature*. **562**, 272–276 (2018).

566 45. B. Pijuan-Sala *et al.*, *Nature*. **566**, 490–495 (2019).

567 46. L. U. Rosen *et al.*, *bioRxiv*, 2009–2022 (2022).

568 47. L. Cong *et al.*, *Science (80-.).* **339**, 819–823 (2013).

569 48. S. J. Clark *et al.*, *Nat. Commun.* (2018), doi:10.1038/s41467-018-03149-4.

49. H. Pages *et al.*, *Bioconductor*. **18129** (2013).

50. R. Argelaguet *et al.*, *Nature*. **576**, 487–491 (2019).

51. A. Liaw, M. Wiener, Title Breiman and Cutler's Random Forests for Classification and Regression Description Classification and regres-sion based on a forest of trees using random inputs (2015).